Journal of Structural Geology 48 (2013) 153–161

Contents lists available at SciVerse ScienceDirect

Journal of Structural Geology

journal homepage: www.elsevier.com/locate/jsg

A new three-dimensional method of fault reactivation analysis

Henri Leclère*, Olivier Fabbri

UMR CNRS 6249, Université de Franche-Comté, 16 route de Gray, 25030 Besançon cedex, France

ARTICLE INFO

Article history:
Received 27 January 2012
Received in revised form
7 November 2012
Accepted 11 November 2012
Available online 26 November 2012

Keywords:
Fault
Stress field
Reactivation
Mohr space
Tohoku-Oki earthquake
Asperity

ABSTRACT

A 3-D method to evaluate the reactivation potential of fault planes is proposed. The method can be applied to cohesive or noncohesive faults whatever their orientation and without any conditions on the regional stress field. It allows computation of the effective stress ratio σ'_3/σ'_1 required to reactivate any fault plane and to determine whether the plane is favorably oriented, unfavorably oriented or severely misoriented with respect to the ambient stress field. The method also includes a graphical sorting tool that involves plotting poles of fault planes on stereoplots for which the boundaries separating the three domains corresponding to favorable orientations, unfavorable orientations and severe misorientations cases are shown. The delineation of these domains is based on the value of the σ'_3/σ'_1 ratio that depends on the orientation of the fault plane with respect to the principal stress axis orientations, the stress shape ratio ($\Phi = (\sigma_2 - \sigma_3)/(\sigma_1 - \sigma_3)$), the coefficient of static friction μ_s of the fault, and the fault cohesion C_0. The method is applied on 145 focal mechanisms of the 2011 March 11th Tohoku-Oki (Japan) earthquake sequence. This application delineates, along or in the vicinity of the Pacific-Okhotsk plate interface, three types of domains characterized by favorable orientations, unfavorable orientations or severe misorientations of mainshock/aftershock fault planes. Aftershock focal mechanisms that plot in the 'severe misorientation' domains are interpreted to have occurred because of pore fluid pressures exceeding the regional minimum principal stress at those locations. The distribution of these 'severe misorientation' domains partly overlaps the asperities or the low-velocity anomalies mapped on the plate interface off NE Japan. The proposed 3-D fault reactivation analysis appears complementary to geophysical investigations.

1. Introduction

The mechanical control of fault reactivation is a very important issue for understanding earthquake hazard (McKenzie, 1969; Scholz, 1998). For three decades, researchers have developed methods directly derived from the Mohr–Coulomb theory and focused on estimating the reactivation potential of pre-existing faults.

The first method, introduced by Sibson (1985), consists of a 2-D analysis that computes the effective stress ratio $R = \sigma'_1/\sigma'_3$ required to reactivate a fault plane. To be reactivated, the fault plane must reach the reactivation envelope governed by the Coulomb criterion ($\tau = \mu_s\, \sigma_n$) where τ is the shear stress on the pre-existing plane, μ_s the coefficient of static friction and σ_n the normal stress acting on the pre-existing plane (Fig. 1a). The 2-D fault reactivation analysis requires knowledge of the angle θ_r between the fault plane and the maximum principal stress σ_1. It is also limited to cases for which the intermediate principal stress axis σ_2 is in the fault plane. Lastly, it assumes that faults are cohesionless.

Depending on the value of the effective stress ratio, R, Sibson (1985) introduced three classes of fault orientations. (1) "Favorably oriented" faults have R values between the minimal R-value ($R_{optimal}$) and ($R_{optimal} \times 1.5$) (Fig. 1a, case (1) and (2)). (2) "Unfavorably oriented" faults have R values larger than 1.5 $R_{optimal}$ (Fig. 1a, case (3)). (3) "Severely misoriented" faults have negative R values (Fig. 1a, case (4)). A negative R value indicates that the magnitude of the minimum principal effective stress is negative ($\sigma'_3 = \sigma_3 - p_f < 0$) and implies that fault reactivation is possible only if the pore fluid pressure p_f is larger than the magnitude of the minimum principal stress ($p_f > \sigma_3$). This 2-D fault reactivation analysis emphasizes the role played by coefficient of static friction along with pore fluid pressure on reactivation of unfavorably oriented or severely misoriented faults, which has been shown in a number of case studies (Collettini and Sibson, 2001; Sibson, 2009; Konstantinou et al., 2011).

To evaluate the reactivation potential of fault planes that do not contain the σ_2 axis, Morris et al. (1996) developed a fault-

* Corresponding author. Tel.: + 33 3 81 66 60 51; fax: +33 3 81 66 65 58.
E-mail address: henri.leclere@univ-fcomte.fr (H. Leclère).

0191-8141/$ – see front matter © 2012 Elsevier Ltd. All rights reserved.
http://dx.doi.org/10.1016/j.jsg.2012.11.004

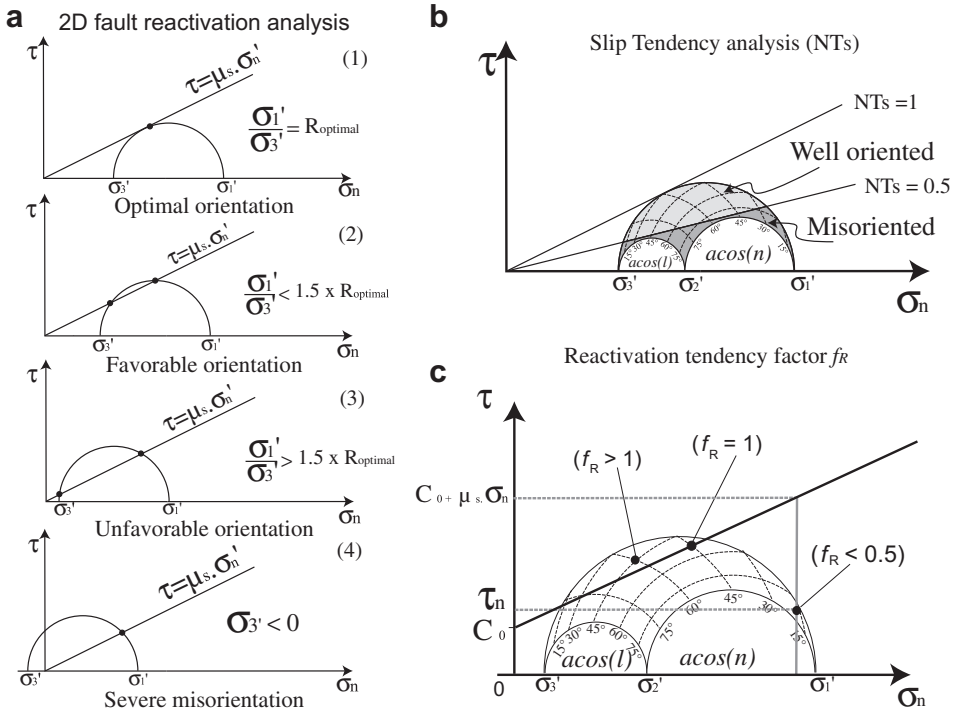

Fig. 1. Mohr diagrams corresponding to different fault-reactivation analyses. (a) Mohr diagrams of the 2-D fault reactivation analysis (Sibson, 1985). (b) Mohr diagram illustrating the Slip-Tendency method (NT_s) where the (σ'_1, σ'_3) Mohr circle is tangent to the reactivation envelope. In the inner circles, *acos* stands for the *inverse cosinus function*. (c) Mohr diagram illustrating the reactivation-tendency factor f_R. In the inner circles, *acos* stands for the *inverse cosinus function*. The reactivation envelope is governed by the Mohr–Coulomb failure criterion and the reactivation tendency factor f_R corresponds to the ratio $\tau_n/(C_0 + \mu_s\sigma_n)$.

reactivation characterization method named slip tendency. The slip tendency method estimates the reactivation potential for any fault plane whatever its orientation with respect to the orientation of the principal stress axes. It uses a 3-D Mohr–Coulomb diagram (Fig. 1b) and knowledge of the reactivation envelope to calculate the stress ratio $T_s = \tau/\sigma_n$ to reactivate any fault plane without knowing the magnitude of the principal stress components. In fact, the T_s value can be calculated by knowing only the orientation of the three principal stress axes and the stress shape ratio $\Phi = (\sigma_2-\sigma_3)/(\sigma_1-\sigma_3)$ (see Neves et al., 2009 for further details). To estimate the ability of a fault to be reactivated under a given stress state, Morris et al. (1996) normalized the slip tendency on any surface with the maximum possible slip tendency Ts_{max}. The normalizing ratio is called NT_s and is equal to T_s/Ts_{max}. A NT_s ratio between 1 and 0.5 indicates that the fault plane is well oriented with respect to the ambient stress field whereas a NT_s ratio less than 0.5 indicates that the fault plane is misoriented. The NT_s method has been applied on seismic sequences or on fault systems (Ventura and Vilardo, 1999; Lisle and Srivastava, 2004; Worum et al., 2004; Collettini and Trippetta, 2007; De Paola et al., 2007; Moeck et al., 2009; Neves et al., 2009; Massironi et al., 2011). Although the NT_s method is applicable to fault planes with any orientation, it does not account for the fault cohesion and, unlike the 2-D method, it cannot identify those fault planes, which can be reactivated only with fluid overpressure ($p_f > \sigma_3$).

To account for the cohesive strength of pre-existing planes, Tong and Yin (2011) extended the work of Morris et al. (1996) by introducing a new parameter, the reactivation-tendency factor $f_R = \tau_n/(C_0 + \mu_s\,\sigma'_n)$, where τ is the shear stress acting on the pre-existing plane and $(C_0 + \mu_s\,\sigma'_n)$ is the critical shear stress required to reactivate a pre-existing cohesive fault plane (Fig. 1c). A reactivation-tendency factor f_R larger or equal to 1 indicates that the pre-existing plane is well oriented with respect to the ambient stress field and can be reactivated, whereas a f_R value below 0.5 indicates that the fault plane is misoriented.

In this study, we extend the analyses of Sibson (1985), Morris et al. (1996) and Tong and Yin (2011) by introducing a general fault reactivation method named 3-D fault reactivation analysis. This method allows evaluation of the reactivation potential for a fault plane without any prerequisite information about the orientations of the regional stress tensor axes with respect to the fault plane or to the Earth's surface. In particular, an Andersonian stress state (one principal stress axis vertical) need not be hypothesized. The method also incorporates cohesion and the coefficient of static friction into the analysis as well as the pore fluid pressure in the fault zone. Application of this method to the Tohoku-Oki (Japan) mainshock/aftershocks seismic sequence as an example provides information about the pore fluid pressures along or in the vicinity of the plate interface.

2. 3-D fault reactivation analysis

2.1. First step: derivation of basic equations

The reactivation of fault planes follows the Mohr–Coulomb failure criterion (Jaeger et al., 2007):

$$\tau = C_0 + \mu_s\left(\sigma_n - P_f\right) \tag{1}$$

where C_0 is the cohesive strength of the fault plane and p_f is the pore fluid pressure.

If the fault plane is cohesionless, Equation (1) can be written as:

$$\tau = \mu_s\left(\sigma_n - P_f\right) \tag{2}$$

If the magnitudes and orientations of the principal effective stresses ($\sigma'_1 = (\sigma_1 - P_f) > \sigma'_2 = (\sigma_2 - P_f) > \sigma'_3 = (\sigma_3 - P_f)$) are known, the shear stress and the effective normal stress acting on a plane are given by the formulae (Jaeger et al., 2007):

$$\tau^2 = (\sigma'_1 - \sigma'_2)^2 l^2 m^2 + (\sigma'_2 - \sigma'_3)^2 m^2 n^2 + (\sigma'_3 - \sigma'_1)^2 l^2 n^2 \quad (3)$$

and

$$\sigma'_n = l^2 \sigma'_1 + m^2 \sigma'_2 + n^2 \sigma'_3 \quad (4)$$

where l, m and n are the direction cosines between the normal n to the fault plane and the principal stress axes σ_1, σ_2 and σ_3 respectively.

To calculate the direction cosines l, m and n for any possible orientation of the σ_1, σ_2 and σ_3 axes, we compute the Cartesian components of the normal n of the given fault plane in a geographic coordinate system (x, y, z as North, East, down) using the following formulae:

$$n_x = -\sin(\delta_n) \cdot \cos(\theta_n) \quad (5)$$

$$n_y = -\sin(\delta_n) \cdot \sin(\theta_n) \quad (6)$$

$$n_z = \cos(\delta_n) \quad (7)$$

where δ_n is the dip angle between the Earth surface and the fault plane, and θ_n is the angle (measured clockwisely) between the x axis and the dip direction of the fault plane.

The Cartesian components of the σ_1, σ_2 and σ_3 axes in the geographic system (x, y, z as North, East, down) are then computed by using the following formulae:

$$x_i = \cos(\delta_i) \cdot \cos(\theta_i) \quad (8)$$

$$y_i = \cos(\delta_i) \cdot \cos(\theta_i) \quad (9)$$

$$z_i = \sin(\delta_i) \quad (10)$$

where $i = 1$, 2, and 3 for the σ_1, σ_2, and σ_3 axes respectively, δ_i is the plunge angle of the σ_i axis and θ_i is the angle measured clockwisely between the x axis and the azimuth of the σ_i axis.

Finally, the direction cosines l, m and n can be computed by using the following formulae:

$$l = \frac{x_1 \cdot n_x + y_1 \cdot n_y + z_1 \cdot n_z}{\sqrt{(x_1^2 + y_1^2 + z_1^2) \cdot \left(n_x^2 + n_y^2 + n_z^2\right)}} \quad (11)$$

$$m = \frac{x_2 \cdot n_x + y_2 \cdot n_y + z_2 \cdot n_z}{\sqrt{(x_2^2 + y_2^2 + z_2^2) \cdot \left(n_x^2 + n_y^2 + n_z^2\right)}} \quad (12)$$

$$n = \frac{x_3 \cdot n_x + y_3 \cdot n_y + z_3 \cdot n_z}{\sqrt{(x_3^2 + y_3^2 + z_3^2) \cdot \left(n_x^2 + n_y^2 + n_z^2\right)}} \quad (13)$$

Equations (3) and (4) can be used only if the magnitudes and orientations of the principal stresses σ'_1, σ'_2 and σ'_3 are known. In most cases, the absolute magnitudes of the principal stresses are unknown. However, their relative magnitudes, expressed by the stress shape ratio Φ, can be determined by inversion methods based on calcite twin inversion (Laurent et al., 1981) or fault-slip data and focal-mechanism stress inversion (Carey and Brunier, 1974; Angelier, 1979; Gephart and Forsyth, 1984; Michael, 1984, 1987; Delvaux and Sperner, 2003; Zalohar and Vrabec, 2010).

Using the stress shape ratio Φ and the effective stress ratio $Q = \sigma'_3/\sigma'_1$, σ'_2 and σ'_3 can be expressed as functions of σ'_1:

$$\sigma'_3 = \sigma'_1 Q \quad (14)$$

$$\sigma'_2 = \sigma'_1 [\Phi(1 - Q) + Q] \quad (15)$$

By substituting Equations (14) and (15) in Equations (3) and (4), the shear stress τ and the effective normal stress σ'_n can be expressed as:

$$\tau^2 = \sigma_1^{2\prime} \Big[(1 - (\Phi(1 - Q) + Q))^2 l^2 m^2 + (\Phi(1 - Q))^2 m^2 n^2 + (Q - 1)^2 l^2 n^2 \Big] \quad (16)$$

$$\sigma_n = \sigma'_1 \left(l^2 + (\Phi(1 - Q) + Q) m^2 + Q n^2 \right) \quad (17)$$

The reactivation of a pre-existing cohesion fault plane must satisfy the Mohr–Coulomb criterion (see Equation (2)), which can be rewritten as:

$$\mu_s = \frac{\tau - C_0}{\sigma_n} \quad (18)$$

Combining Equations (16)–(18) gives:

$$\mu_s = \frac{\sqrt{(1 - (\Phi(1 - Q) + Q))^2 l^2 m^2 + (\Phi(1 - Q))^2 m^2 n^2 + (Q - 1)^2 l^2 n^2} - \dfrac{C_0}{\sigma'_1}}{l^2 + (\Phi(1 - Q) + Q) m^2 + Q n^2} \quad (19)$$

which can be rewritten as:

$$\mu_s = \frac{\sqrt{Q^2 C - 2QC + C} - \dfrac{C_0}{\sigma'_1}}{Q \cdot A + B} \quad (20)$$

where

$$A = m^2 + n^2 - \Phi m^2 \quad (21)$$

$$B = l^2 + \Phi m^2 \quad (22)$$

$$C = (1 - \Phi)^2 l^2 m^2 + \Phi^2 n^2 m^2 + l^2 n^2 \quad (23)$$

The expression of Q as a function of l, m, n, Φ, and C_0/σ_1 is a second-degree polynomial function

$$Q^2\left(A^2\mu_s^2 - C\right) + Q(2\cdot A\cdot D\cdot\mu_s + 2C) + D^2 - C = 0 \quad (24)$$

with

$$D = B\cdot\mu_s + \frac{C_0}{\sigma_1'} \quad (25)$$

which can be solved as follows:

$$\Delta = (2A\cdot D\cdot\mu_s + 2C)^2 - 4\left(A^2\mu_s^2 - C\right)\left(D^2 - C\right) \quad (26)$$

$$Q = \frac{-(2A\cdot D\cdot\mu_s + 2\cdot C) \pm \sqrt{\Delta}}{(A^2\mu_s^2 - C)} \quad (27)$$

with

$$\{Q \in \mathbb{R}; Q \le 1\}$$
$$\{\mu_s \in \mathbb{R}; 0 \le \mu_s\}$$

According to Equation (27), Q values range between $-\infty$ and Q_{max}, with $Q_{max} = 1$ and is obtained when $\sigma_1' = \sigma_3'$. $Q_{optimal}$ is defined in Equation (28).

2.2. Second step: construction of contoured Q-value stereoplots

To construct a Q-value stereoplot, the orientations of the principal stress axes and the values of Φ, C_0/σ_1 and μ_s must be fixed. Fig. 2a shows an example of a Q-value stereoplot computed for a horizontal N–S σ_1 axis, a vertical σ_2 axis, a horizontal E–W σ_3 axis, a Φ ratio of 0.5, a C_0/σ_1 ratio of 0 and a coefficient μ_s of 0.6. For any plane (defined by its strike and dip angle), the Q ratio is computed and its value is then attributed to the pole of the plane on the stereoplot. This operation is then repeated for all strikes between 0 and 360° and for all dip angles between 0 and 90°. The obtained Q-value distribution on the stereoplot is then contoured (Fig. 2a) using the Matlab® *contour* function.

2.3. Third step: delineation of favorable orientation, unfavorable orientation and severe misorientation domains

The three *favorable orientation*, *unfavorable orientation* and *severe misorientation* domains of Sibson (1985) can be delineated on the Q-value stereoplot (Fig. 2b). The *favorable orientation* domain contains Q values comprised between $Q_{optimal}$ and half of $Q_{optimal}$, where $Q_{optimal}$ is given by:

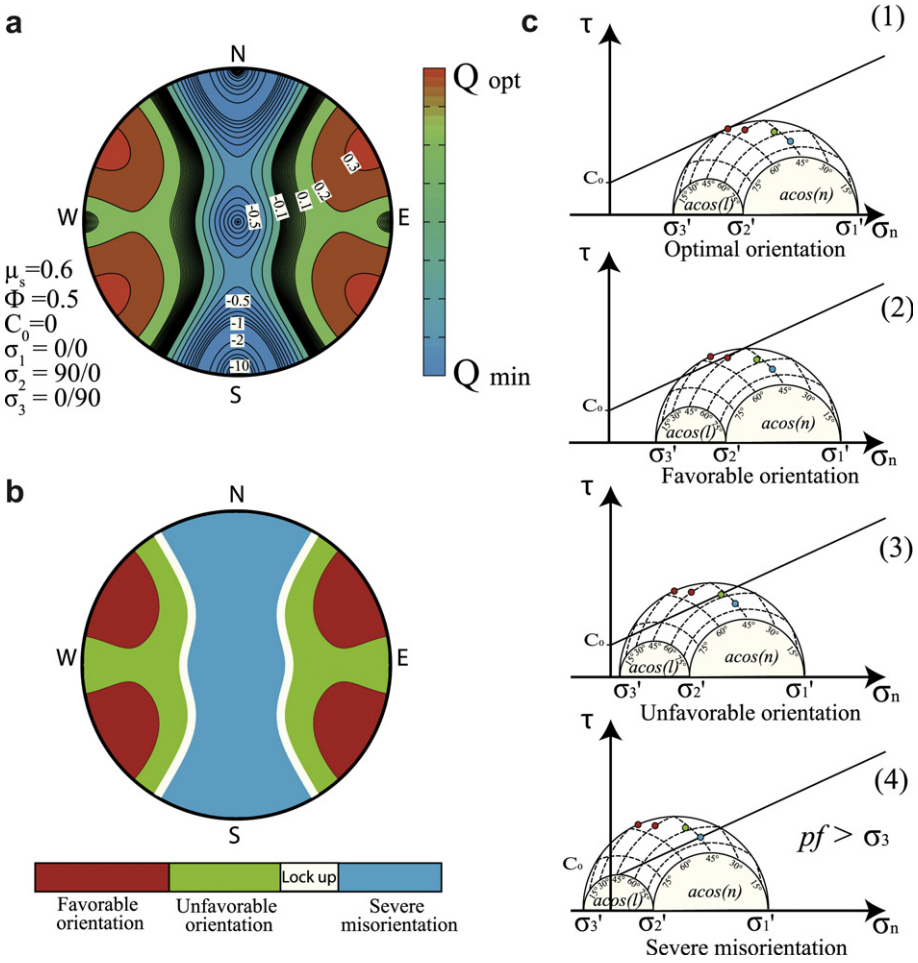

Fig. 2. Representation of the 3-D fault reactivation analysis. (a) Lower-hemisphere equal-area stereoplot of contoured Q values. (b) Lower-hemisphere equal-area stereoplot displaying the three classes (favorable orientation, unfavorable orientation and severe misorientation). The lock-up corresponds to the limit between the unfavorable orientation domain and the severely misoriented domain when Q tends toward zero. (c) Mohr diagrams showing the reactivation of four representative fault planes: (1) optimal fault orientation for which the (σ_1, σ_3) circle is tangent to the reactivation envelope (red dot); (2) favorably oriented fault (red dot); (3) unfavorably oriented fault (green dot); (4) severely misoriented fault (blue dot). The reactivation envelope in the four cases has the same coefficient of friction μ_s and cohesive strength C_0. In case (3), the reactivation of the plane is possible even if $\sigma_3' > 0$. In case (4), the reactivation is possible only if $\sigma_3' < 0$, such that is $p_f > \sigma_3$.

$$Q_{optimal} = \frac{1 - \mu_s \cdot \tan(\theta_r) - \dfrac{C_0}{\sigma_1 \cdot \sin(\theta_r) \cdot \cos(\theta_r)}}{1 + \mu_s \cdot \cot(\theta_r)} \quad (28)$$

The angle θ_r is the angle between the σ_1 axis and the optimally oriented fault plane in the sense of Sibson (1985) and is given by:

$$\theta_r = 0.5 \tan^{-1}\left(\frac{1}{\mu_s}\right) \quad (29)$$

On a Mohr diagram, the $Q_{optimal}$ case corresponds to a (σ'_1, σ'_3) Mohr circle tangent to the reactivation envelope (Fig. 2c, case (1)), and any favorable orientation fault will plot close to the tangent position (Fig. 2c, case (2)).

The *unfavorable orientation* domain contains the Q values comprised between two-third of $Q_{optimal}$ and zero. On a Mohr diagram, unfavorably oriented faults will plot as illustrated on Fig. 2c (case (3)).

Lastly, the *severe misorientation* domain is characterized by negative Q values, implying that fault reactivation is possible only for pore fluid pressures p_f larger than σ_3. The limit, or "lock-up", placed by Sibson (1985) between the *unfavorable orientation* domain and the *severe misorientation* domain corresponds to Q values close to zero (Fig. 2b). On a Mohr diagram, severely misoriented faults require a negative σ'_3 (Fig. 2c, case (4)).

The 'domain-bearing' Q value stereoplots such as depicted in Fig. 2b provide a simple and straightforward means to evaluate the reactivation potential of a fault plane. If the orientations of the principal stress axes and the Φ, C_0/σ_1 and μ_s values are known (or inferred), plotting the pole of a given fault plane on the corresponding stereoplot indicates the capability of the fault plane to reactivate, while determining the appropriate stress state for the fault in terms of the domains (*favorable orientation*, *unfavorable orientation* or *severe misorientation*). The Matlab® script used for drawing stereoplots such as the one depicted in Fig. 2a can be obtained from the corresponding author.

2.4. Influence of stress tensor characteristics or fault properties on the aspect of the 'domain-bearing' Q-value stereoplots

Fig. 3 shows an example of a set of 'domain-bearing' Q value stereoplots computed for particular stress tensor characteristics (principal stress axis orientations and Φ values) and for particular fault properties (C_0/σ_1 and μ_s values). The three stereoplots corresponding to the three possible Andersonian stress tensors (one vertical principal stress axis) are located at the summits of the central triangle of Fig. 3. The three triangles adjacent to the central triangle (i.e., sharing two summits with the central triangle) correspond to non-Andersonian stress tensors for which two principal stress axes are tilted by 45° around the horizontal principal stress axis. These 6 stereoplots correspond to Φ, C_0/σ_1 and μ_s values respectively equal to 0.5, 0.1 and 0.6. For each of these 6 cases, 6 additional stereoplots are computed, for which the orientations of the stress axes are *not modified*, but for which the Φ, C_0/σ_1 and μ_s values vary as indicated: Φ is equal either to 0.15 or 0.85, C_0/σ_1 is equal either to 0 or 0.1, and μ_s is equal either to 0.15 or 0.85. The choice of these values is justified as follows. The three values of Φ correspond to representative stress tensor configurations such as σ_2 close to σ_3 ($\Phi = 0.15$), σ_2 "half-way" between σ_1 and σ_3 ($\Phi = 0.5$, i.e., $\sigma_2 = (\sigma_1 + \sigma_3)/2$), and σ_2 close to σ_1 ($\Phi = 0.85$). Following Byerlee (1978), the three tested values of μ_s correspond to the largest rock friction coefficients commonly encountered in the Earth's crust (0.85), to a moderate yet common friction (0.6) and to a weak friction (0.15). The zero value for C_0/σ_1 corresponds to a cohesionless fault. The 0.1 value corresponds to cases for which the C_0 value is 10% of σ_1. At seismogenic depths (5–20 km) in the continental crust, the order of magnitude of σ_1 is 100 MPa (e.g., Engelder, 1993; Magee and Zoback (1993)), whereas that of C_0 does not depend on depth and is a few tens of MPa (Goodman, 1989; Jaeger et al., 2007). The difference in the orders of magnitude explains the 0.1 value for C_0/σ_1.

Each of the 42 stereoplots depicted on Fig. 3 displays the three *favorable orientation*, *unfavorable orientation* and *severe misorientation* domains. Fig. 3 shows how these domains change on the

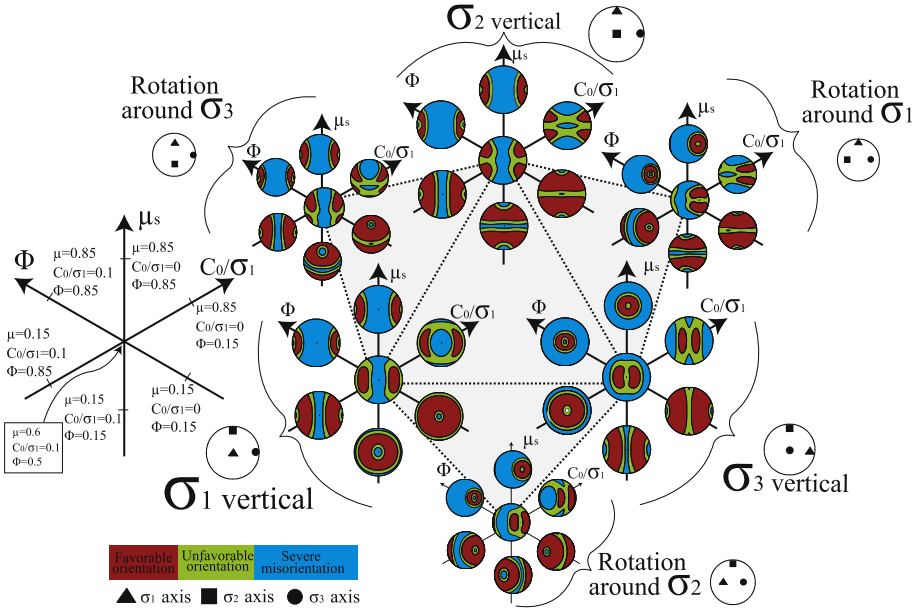

Fig. 3. Stereoplots for application of the 3-D fault reactivation analysis. Six sets of seven stereoplots are presented where each set illustrates the slip-tendency domains for seven combinations of C_0/σ_1, μ_s and Φ. Specific values used are $C_0/\sigma_1 = 0$ or 0.1, $\mu_s = 0.15$, 0.6 or 0.85, and $\Phi = 0.15$, 0.5 or 0.85. As labeled, three of the sets are for different Andersonian cases where one principal stress is vertical. The other three sets are for cases where no principal stress is vertical and instead, two principal stresses are rotated by 45° about one of the horizontal principal stresses.

equal-area plots when one or several of the stress tensor characteristics or fault properties vary. It shows that the 3-D fault reactivation analysis can be applied to any geological stress tensor and to any fault properties. Drawing a series of stereoplots such as those depicted in Fig. 3 (the Matlab® script used for drawing the stereoplots of Fig. 3 can be obtained from the corresponding author) can help exploring the influence of one parameter, for instance μ_s, on the mechanical behavior of a fault population. By drawing stereoplots for discrete values of μ_s between for instance 0.2 and 0.7 (e.g., 0.2, 0.3, 0.4, 0.5, 0.6, 0.7) and by plotting the poles of the faults on the stereoplots, one can obtain an insight on how the distribution of the favorably oriented, unfavorably oriented or severely misoriented faults varies with μ_s. The distribution obtained from stereoplots can then be plotted on as many maps as μ_s values, to gain further insights about the spatial distribution of the three domains. An example of such an analysis is given in the next section.

3. Application of the 3-D fault reactivation method on the 2011 Tohoku-Oki earthquake sequence

To illustrate the usefulness of the proposed method, this section presents an analysis of the 2011 Tohoku-Oki seismic sequence (mainshock and aftershocks). This analysis provides an insight about the mechanical state of the Pacific-Okhotsk plate interface. More precisely, it shows that the interface is heterogeneous and that, depending on the retained fault properties, some areas ('patches') may be characterized by overpressured pore fluids. The distribution of these overpressurized pore fluid patches is in turn compared with that of asperities or low-velocity anomalies deduced from seismological studies.

3.1. Analysis and results

The March 11, 2011, Tohoku-Oki earthquake occurred off the Pacific coast of Northeast Japan and caused a devastating tsunami. The moment magnitude M_w 9.0 mainshock was followed by a sequence of aftershocks whose focal mechanisms are provided by the F-net seismological network (http://www.fnet.bosai.go.jp/) of the National Research Institute for Earth Science and Disaster Prevention (NIED; Fig. 4). The 3-D fault reactivation analysis is applied to the focal mechanisms of the Tohoku-Oki mainshock and to 324 aftershocks occurring between March 11, 2011 and June 21, 2011 and whose M_w magnitudes are larger than 5. The 324 focal-mechanism database is considered to be representative of the Tohoku-Oki earthquake aftershock sequence.

The first step in the analysis is to determine the orientation of the principal stress axes and the stress shape ratio Φ for the Japan Trench seismogenic zone. This determination is done by using the focal mechanism data of earthquakes with magnitudes $M_w > 7.0$ having occurred in the vicinity of the plate interface (Fig. 4) and *before* March 11, 2011. The focal mechanism data are extracted from the Global CMT catalog (*http://www.globalcmt.org*) and are analyzed with the WinTensor stress inversion program (Delvaux and Sperner, 2003). This program uses a function (F5; also called f3 in Delvaux and Sperner, 2003) that minimizes both the misfit angle α between the actual slip vector and the theoretical slip vector, and the shear stress/normal stress ratio (τ/σ_n) acting on the fault plane. A small misfit angle α indicates that slip on the fault plane is governed by the regional stress field, whereas a large misfit angle α indicates that slip is not governed by the regional stress field but more likely by local stress perturbations. The magnitudes of the shear stress τ and of the normal stress σ_n provide an indication about the slip tendency for the faults. A plane with a small σ_n magnitude and a large τ magnitude is more easily reactivated than a plane with a large σ_n magnitude and a small τ magnitude. The function F5 varies between 0 and infinity. A small F5 value indicates that the fault is governed by the regional stress field and has a favorable tendency to slip.

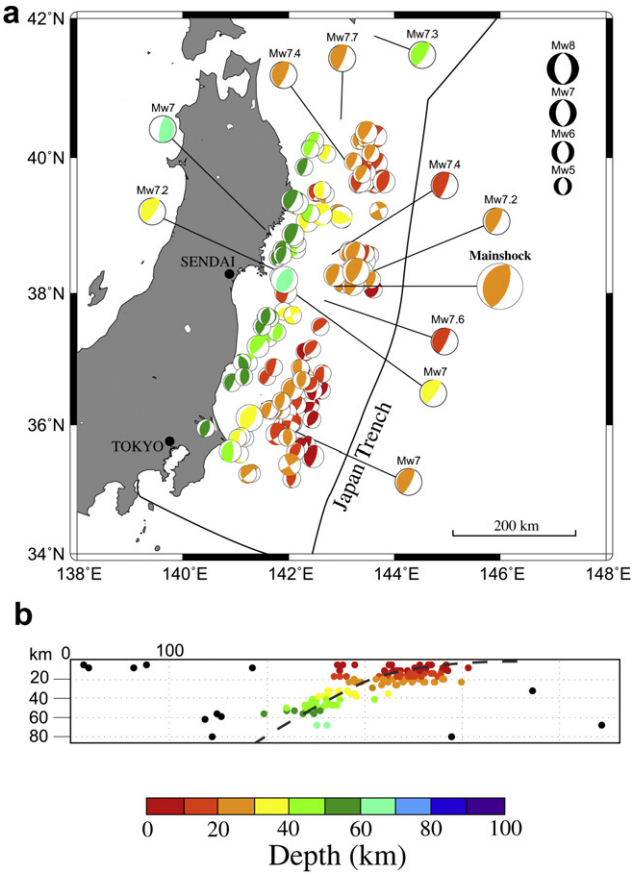

Fig. 4. (a) Focal mechanisms of the 145 selected earthquakes from the 2011 Tohoku-Oki mainshock/aftershock earthquake sequence used for this analysis. Also plotted are the 10 focal mechanisms for large earthquakes ($M_w > 7$) that occurred prior to the Tohoku-Oki mainshock, providing regional stress information. (b) Section across the subduction zone showing the selected focal mechanisms colored for depth and 12 focal mechanisms with black dots that are > 40 km above or under the plate interface.

Stress inversion of the ten major precursor earthquakes for the Japan Trench seismogenic zone in the vicinity of the Tohoku-Oki hypocentral area yields a σ_3 axis oriented N279°E and plunging 83°, a nearly horizontal σ_1 axis oriented N124°E and plunging 5°, a nearly horizontal σ_2 axis oriented N34°E and plunging 2°, and a stress shape ratio Φ of 0.4. By using these regional stress tensor characteristics, the misfit angle α and the F5 value of every nodal plane for the 325 focal mechanisms of the Tohoku-Oki aftershock sequence are then computed. From the 325 focal mechanisms, 168 mechanisms have a misfit angle α larger than the threshold value of 30° for either of the nodal planes. This large misfit angle indicates that the reactivation of these 168 planes was not governed by the regional stress field as determined above from the $M > 7$ events, but more likely we believe to have been triggered by local stress perturbations resulting from the main shock or from pre-existing faults or other material heterogeneities in the rock volume.

Stress perturbations are reported from various seismological analyses of the Tohoku-Oki mainshock (Hasegawa et al., 2011; Ide et al., 2011; Yoshida et al., 2012). They include aftershocks showing normal fault-type focal mechanisms despite fault plane geometries which are interpreted to result from dynamic overshoot of the Tohoku-Oki main rupture (Ide et al., 2011). The fault planes of

the 157 remaining focal mechanisms are the nodal planes having the smallest F5 values. Among these remaining mechanisms, and based on available focal depths (http://www.fnet.bosai.go.jp/), 145 events are located in the vicinity (<20 km) of the NE Japan plate interface (Fig. 4b). To the contrary, 12 events located >20 km above or under the plate interface may be considered to be not directly related to interplate seismicity (Hayes et al., 2009), excluding them from the analysis.

The 145 earthquake fault planes are then evaluated for their predicted expectation for reactivation. The 3-D fault reactivation analysis requires knowledge of l, m, n, μ_s, C_0/σ_1 and Φ values. The l, m, n and Φ values are determined by using the orientations of the σ_1, σ_2 and σ_3 axes and the stress shape ratio calculated from the inversion of ($M_w > 7$) earthquake population. The ratio C_0/σ_1 is equal to zero due to the unknown magnitudes of σ_1 and C_0. Given the values of l, m, n, Φ and C_0/σ_1, the Q values required to reactivate the 145 faults are computed for four coefficients of static friction ($\mu_s = 0.2, 0.4, 0.6, 0.8$) in order to consider the possible influence of the material strength on fault reactivation. The epicenters of the 145 faults are plotted on a map along with their Q values to define the areas (along the plate interface) where the faults are favorably oriented, unfavorably oriented or severely misoriented (Fig. 5). To delineate these areas, a colored dot is assigned to each epicenter as function of the corresponding Q value, and the dots are then contoured by using a Gaussian smoothing (Fig. 5). The Gaussian interpolation method allows one to produce a smooth image from

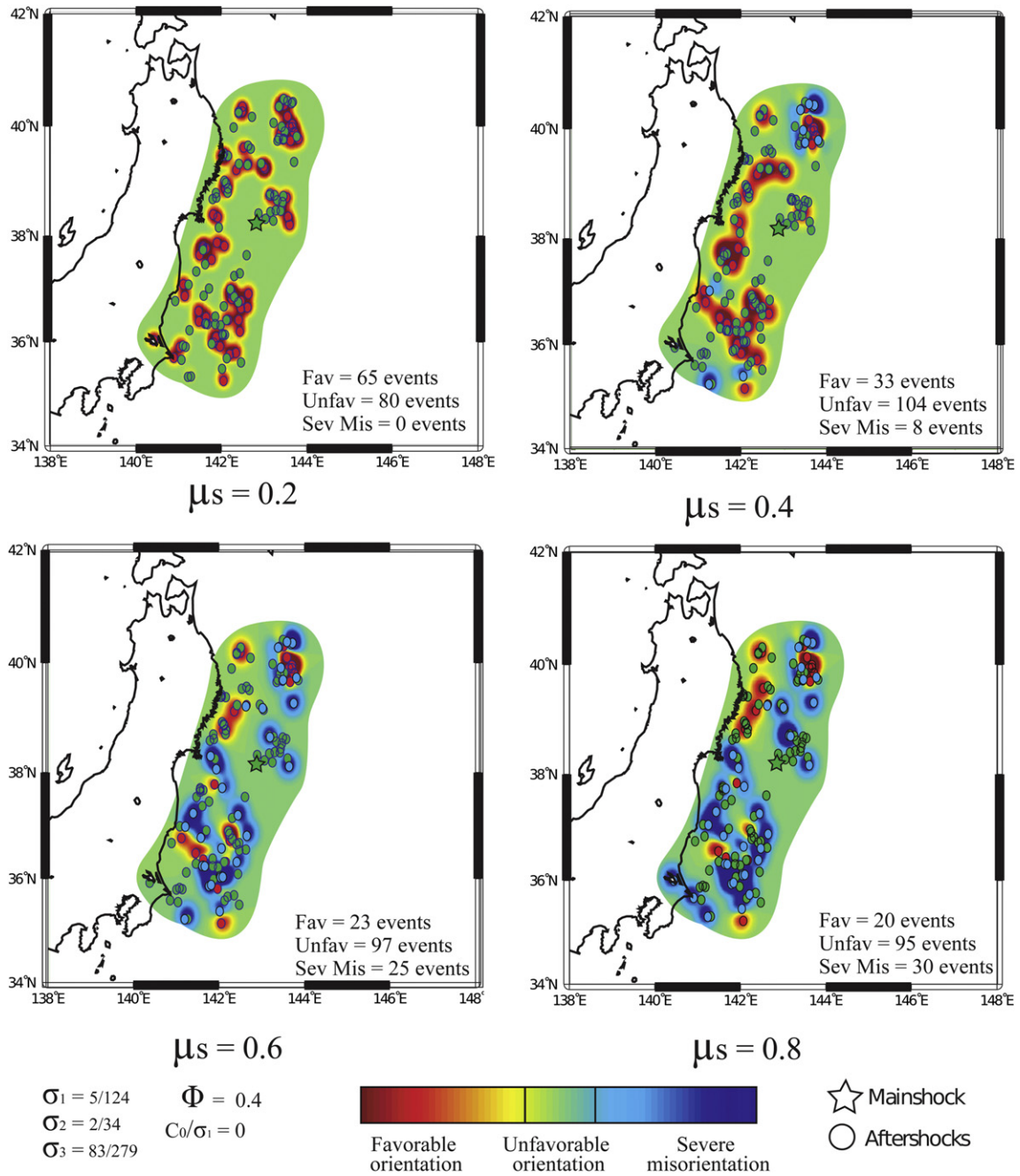

Fig. 5. Spatial distribution of the areas where the faults are optimally oriented (red), misoriented (green) and severely misoriented (blue) along the plate interface for four values of coefficient of static friction. The points correspond to the 145 epicenters of earthquakes located along the plate interface.

irregularly scattered data. The smoothing is done by weighting the scattered data based on their distance to a considered point. The weighting decreases non-linearly with distance but following a Gaussian function. The smooth image emphasizes the values of close data rather than those of remote data. This smoothing may artificially introduce 'unfavorable orientation' domains (green domains on Fig. 5) between 'favorable orientation' domains and 'severe misorientation' domains even if no epicenter corresponding to an unfavorably oriented fault-linked focal mechanism (i.e., green dot) lies between. However, the delineation of the 'favorable orientation' domains or 'severe misorientation' domains is not modified by the smoothing.

3.2. Discussion

If weak materials with static friction coefficients $\mu_s = 0.2–0.4$ are assumed along the NE Japan plate interface as for some other crustal faults (Morrow et al., 1992; Saffer and Marone, 2003; Moore and Rymer, 2007; Ikari et al., 2011; Lockner et al., 2011), the number of severely misoriented faults drops to zero. Indeed, only 8 faults (6%) appear as severely misoriented for a static friction of 0.4, while no fault is severely misoriented for a static friction of 0.2 (Fig. 5). However, laboratory experiments show that small values of friction coefficients are predominantly obtained for hydrated clay minerals such as smectite and for olivine alteration minerals such as talc or serpentine. Given the likely occurrence of dehydration reactions, smectite cannot be present at the depths of nucleation of the Tohoku-Oki earthquake mainshock/aftershock sequence and is likely to be replaced by dehydrated minerals with larger friction coefficient values (Morrow et al., 1992; Saffer and Marone, 2003; Ikari et al., 2007; Behnsen and Faulkner, 2012). Similarly, the Japan Trench is characterized by clastic sedimentation where quartz and clay minerals predominate, and talc or serpentine is neither reported nor suggested by any observation (Von Huene et al., 1994; Takahashi et al., 2000; Tsuru et al., 2000, 2002; Miura et al., 2005). Consequently, small friction (0.2–0.4) material properties cannot be invoked to explain the reactivation of unfavorably oriented or severely misoriented fault planes. Conversely, the reactivation of these planes can be explained by fluid overpressures. The presence of overpressured fluids along the plate interface has been suggested by a Mohr–Coulomb mechanical analysis conducted by Hasegawa et al. (2011). These authors also estimated a pore pressure ratio λ_v on the NE Japan plate interface close to ~0.94 (pore fluid pressure close to lithostatic conditions). Though located further north of the 2011 Tohoku-Oki epicenter, the rupture area of the 1968 Tokachi-Oki earthquake (M 8.2) was also characterized by elevated pore pressures along the plate interface, as suggested by a stress tensor analysis of the aftershock sequence carried out by Magee and Zoback (1993).

The reactivation of the *severely misoriented* fault planes requires fluid pressures exceeding the magnitude of the least principal stress component ($p_f > \sigma_3$). The 'severely misoriented' domains (Fig. 5) are interpreted to result from the local fluid abundance triggering overpressure along or near the plate interface during the Tohoku-Oki earthquake sequence. These domains, or patches, could correspond to rock volumes characterized by permeabilities and/or porosities different from those in the surrounding volumes (corresponding to the 'favorable orientation' domains). These patches are reminiscent of the low-velocity anomalies at or near the NE Japan plate interface deduced from P-wave (V_P) tomographic investigations carried out by Zhao et al. (2011). The low-V_P patches are interpreted to contain subducted sediments and fluids associated with slab dehydration. The distribution of the low-V_P patches (Zhao et al., 2011) partly overlaps that of the 'severely misoriented' domains obtained for $\mu_s = 0.8$ (Fig. 5). Similarly, a comparison between Fig. 5 (map for $\mu_s = 0.8$) and the asperity (large slip area) map proposed by Yamanaka and Kikuchi (2004) for M7 or larger events suggests that the asperities are located in our 'unfavorably oriented' or 'severely misoriented' domains. Though not conclusive, these comparisons tend to indicate that the NE Japan plate interface is heterogenous and that pore fluid overpressures might be part of the cause of the heterogeneity. It is important to note that the comparisons deal with data obtained by independent methods (focal mechanisms, V_P tomography, strong motion data).

The reactivation of the *unfavorably oriented* fault planes (65% of the analyzed aftershocks) can be explained by pore fluid pressures remaining lower than the magnitude of the least principal stress component ($0 < p_f < \sigma_3$). It can alternatively be explained by an increase of the magnitude of the maximum principal stress component σ_1 following tectonic loading, or by a combination of both mechanisms (fluid pressure increase or tectonic loading). In particular, the reactivation of the Tohoku-Oki mainshock fault plane, which for static friction values not weaker than 0.2, falls in the *unfavorably oriented* domain, can be explained by one of these two mechanisms or by a combination of them.

The 3-D fault reactivation method can be applied to any earthquake sequence (main shock and aftershocks), occurring at plate boundaries or along intra-plate faults. One condition is that the regional stress tensor is known or can be reliably determined. The method should be preferentially applied to those fault zones where pore fluid overpressures are suspected. Indeed, depending on the value of the coefficient of friction, the severely misoriented domains may correspond to parts of the fault that contain pore fluids at pressures exceeding the magnitude of the least principal stress component. Hence, the method can help with identifying overpressured rock volumes.

4. Conclusion

The 3-D fault reactivation analysis is a generalization of the previously published reactivation analysis methods. Unlike the 2-D fault reactivation (Sibson, 1985), the 3-D analysis considers faults with cohesion, and does not require a particular geometry for the σ_2 axis. It also may incorporate the involvement of pore fluid pressure for reactivation of severely misoriented faults.

The 3-D fault reactivation analysis can be applied to any fault plane (Fig. 3). Its originality lies in determining, for any geological setting, the Q values required to reactivate the fault planes and whether fault planes are favorably oriented, unfavorably oriented or severely misoriented with respect to the regional stress field. Moreover, the *severely misoriented* class is particularly interesting because it shows that reactivation is possible only if fluid pressures in excess of the least principal stress component ($p_f > \sigma_3$) exist in the fault zone. This condition is however dependent of the value of the coefficient of friction, which is a controlling parameter. Indeed, for low values of μ_s, all faults can fall in the *favorably oriented* or *unfavorably oriented* classes, and no fault will be *severely misoriented*. In such cases, no conclusions about pore fluid pressures should be drawn.

The 3-D fault reactivation analysis is applied to 145 focal mechanisms of the 2011 Tohoku-Oki mainshock/aftershock sequence in the vicinity of the NE Japan plate interface. The 3-D fault reactivation analysis shows that for a Byerlee-type static friction ($\mu_s = 0.6–0.8$), only 15% of the faults are favorably oriented, while about 20% of the faults are *severely misoriented* and their reactivation requires pore fluid pressures in excess of the least principal stress component ($p_f > \sigma_3$). The overpressured fluid domains appear as patches on the plate interface. The presence of these patches can be attributed to hydraulic heterogeneities such as rocks with contrasted porosities and/or permeabilities. The

remaining 65% of the faults correspond to unfavorably oriented faults (including the mainshock fault plane) and their reactivation was possible by one or by a combination of the two mechanisms: pore fluid pressure build-up in the fault zone but remaining lower than the magnitude of the least principal stress component; $0 < p_f < \sigma_3$, or by an increase of the magnitude of the maximum principal stress component σ_1 following tectonic loading.

In conclusion, the 3-D reactivation analysis is a method that can estimate the ease of reactivation of fault planes for any geological setting. It combines all the possibilities given by the previously published methods and appears to be more sensitive to describe the ability of fault planes to be reactivated.

Acknowledgments

Fig. 4 was prepared using GMT (Wessel and Smith, 1991). Comments from the reviewers (C. Collettini and A. Morris) and a journal editor (W. Dunne) helped clarifying the manuscript.

References

Angelier, J., 1979. Determination of the mean principal directions of stresses for a given fault population. Tectonophysics 56, T17–T26.
Behnsen, J., Faulkner, D.R., 2012. The effect of mineralogy and effective normal stress on frictional strength of sheet silicates. Journal of Structural Geology 42, 49–61.
Byerlee, J., 1978. Friction of rocks. Pure and Applied Geophysics 116, 615–626.
Carey, E., Brunier, B., 1974. Analyse théorique et numérique d'un modèle mécanique élémentaire appliqué à l'étude d'une population de failles. Comptes-Rendus de l'Académie des Sciences série II, 891–894.
Collettini, C., Sibson, R.H., 2001. Normal faults, normal friction? Geology 29, 927–930.
Collettini, C., Trippetta, F., 2007. A slip tendency analysis to test mechanical and structural control on aftershock rupture planes. Earth and Planetary Science Letters 255, 402–413.
De Paola, N., Collettini, C., Trippetta, F., Barchi, M.R., Minelli, G., 2007. A mechanical model for complex fault patterns induced by evaporite dehydration and cyclic changes in fluid pressure. Journal of Structural Geology 29, 1573–1584.
Delvaux, D., Sperner, B., 2003. New aspects of tectonic stress inversion with reference to the tensor program. In: Nieuwland, D.A. (Ed.), New Insights into Structural Interpretation and Modelling. Geological Society, London, Special Publication 212, pp. 75–100.
Engelder, T., 1993. Stress Regimes in the Lithosphere. Princeton University Press, Princeton, New Jersey. 451 p.
Gephart, J., Forsyth, D., 1984. An improved method for determining the regional stress tensor using earthquake focal mechanism data: application to the San Fernando earthquake sequence. Journal of Geophysical Research 89, B11. http://dx.doi.org/10.1029/JB089iB11p09305.
Goodman, R.E., 1989. Introduction to Rock Mechanics, second ed. John Wiley and Sons, New York. 562 p.
Hasegawa, A., Yoshida, K., Okada, T., 2011. Nearly complete stress drop in the 2011 M_w 9.0 off the Pacific coast of Tohoku earthquake. Earth Planets Space 63, 703–707.
Hayes, G., Wald, D.J., Keranen, K., 2009. Advancing techniques to constrain the geometry of the seismic rupture plane on subduction interfaces a priori: higher-order functional fits. Geochemistry, Geophysics, Geosystems 10, Q09006. http://dx.doi.org/10.1029/2009GC002633.
Ide, S., Baltay, A., Beroza, G., 2011. Shallow dynamic overshoot and energetic deep rupture in the 2011 M_w 9.0 Tohoku-Oki Earthquake. Science 332, 1426–1429.
Ikari, M., Saffer, D.M., Marone, C., 2007. Effect of hydration state on the frictional properties of montmorillonite-based fault gouge. Journal of Geophysical Research 112 (B06423). http://dx.doi.org/10.1029/2006JB004748.
Ikari, M.J., Marone, C., Saffer, D.M., 2011. On the relation between fault strength and frictional stability. Geology 39, 83–86.
Jaeger, J.C., Cook, N.G.W., Zimmerman, R., 2007. Fundamentals of Rock Mechanics, fourth ed. Blackwell, Oxford. 475 p.
Konstantinou, K.I., Evangelidis, C.P., Melis, N.S., 2011. The 8 June 2008 M_w 6.4 earthquake in northwest Peloponnese, western Greece: a case of fault reactivation in an overpressured lower crust? Bulletin of the Seismological Society of America 101, 438–445.
Laurent, P., Bernard, P., Vasseur, G., Etchecopar, A., 1981. Stress tensor determination from the study of *e* twins in calcite: a linear programming method. Tectonophysics 78, 651–660.
Lisle, R.J., Srivastava, D.C., 2004. Test of the frictional reactivation theory for faults and validity of fault-slip analysis. Geology 32, 569–572.
Lockner, D.A., Morrow, C., Moore, D., Hickman, S., 2011. Low strength of deep San Andreas fault gouge from SAFOD core. Nature 472, 82–86.
Magee, M.E., Zoback, M.D., 1993. Evidence for a weak interplate thrust fault along the northern Japan subduction zone and implications for the mechanics of thrust faulting and fluid expulsion. Geology 21, 809–812.
Massironi, M., Bistacchi, A., Menegon, L., 2011. Misoriented faults in exhumed metamorphic complexes: rule or exception? Earth and Planetary Science Letters 307, 233–239.
McKenzie, D.P., 1969. The relation between fault plane solutions for earthquakes and the directions of the principal stresses. Bulletin of the Seismological Society of America 59, 591–601.
Michael, A., 1984. Determination of stress from slip data: faults and folds. Journal of Geophysical Research 89, B13. http://dx.doi.org/10.1029/JB089iB13p11517.
Michael, A., 1987. Use of focal mechanisms to determine stress: a control study. Journal of Geophysical Research 92, B1. http://dx.doi.org/10.1029/JB092iB01p00357.
Miura, S., Takahashi, N., Nakanishi, A., Tsuru, T., Kodaira, S., Kaneda, Y., 2005. Structural characteristics off Miyagi forearc region, the Japan Trench seismogenic zone, deduced from a wide-angle reflection and refraction study. Tectonophysics 407, 165–188.
Moeck, I., Kwiatek, G., Zimmermann, G., 2009. Slip tendency analysis, fault reactivation potential and induced seismicity in a deep geothermal reservoir. Journal of Structural Geology 31, 1174–1182.
Moore, D.E., Rymer, M.J., 2007. Talc-bearing serpentinite and the creeping section of the San Andreas fault. Nature 448, 795–797.
Morris, A., Ferrill, D.A., Henderson, D.B., 1996. Slip-tendency analysis and fault reactivation. Geology 24, 275–278.
Morrow, C., Radney, B., Byerlee, J., 1992. Frictional strength and the effective pressure law of montmorillonite and illite clays. In: Fault Mechanics and Transport Properties of Rocks: A Festschrift in Honor of W.F. Brace. Academic Press, San Diego, CA, pp. 69–88 (Chapter 3).
Neves, M., Paiva, L., Luis, J., 2009. Software for slip-tendency analysis in 3D: a plug-in for Coulomb. Computers and Geosciences 35, 2345–2352.
Saffer, D.M., Marone, C., 2003. Comparison of smectite- and illite-rich gouge frictional properties: application to the updip limit of the seismogenic zone along subduction megathrusts. Earth and Planetary Science Letters 215, 219–235.
Scholz, C.H., 1998. Earthquakes and friction laws. Nature 391, 37–42.
Sibson, R.H., 1985. A note on fault reactivation. Journal of Structural Geology 7, 751–754.
Sibson, R.H., 2009. Rupturing in overpressured crust during compressional inversion - the case from NE Honshu, Japan. Tectonophysics 473, 404–416.
Takahashi, N., Kodaira, S., Tsuru, T., Park, J.O., Kaneda, Y., 2000. Detailed plate boundary structure off northeast Japan coast. Geophysical Research Letters 27, 1977–1980.
Tong, H., Yin, A., 2011. Reactivation tendency analysis: a theory for predicting the temporal evolution of preexisting weakness under uniform stress state. Tectonophysics 503, 195–200.
Tsuru, T., Park, J.O., Takahashi, N., Kodaira, S., Kido, Y., Kaneda, Y., Kono, Y., 2000. Tectonic features of the Japan Trench convergent margin off Sanriku, northeastern Japan, revealed by multichannel seismic reflection data. Journal of Geophysical Research 105, 16403–16413.
Tsuru, T., Park, J.O., Miura, S., Kodaira, S., Kido, Y., 2002. Along-arc structural variation of the plate boundary at the Japan Trench margin: implication of interplate coupling. Journal of Geophysical Research 107, 2357–2371.
Ventura, G., Vilardo, G., 1999. Slip tendency analysis of the Vesuvius faults: implications for the seismotectonic and volcanic hazard assessment. Geophysical Research Letters 26, 3229–3232.
Von Huene, R., Klaeschen, D., Cropp, B., Miller, J., 1994. Tectonic structure across the accretionary and erosional parts of the Japan Trench margin. Journal of Geophysical Research 99, 22349–22361.
Wessel, P., Smith, W.H.F., 1991. Free software helps map and display data. EOS Transactions, AGU 72, 441.
Worum, G., van Wees, J., Bada, G., van Balen, R.T., Cloetingh, S., Pagnier, H., 2004. Slip tendency analysis as a tool to constrain fault reactivation: a numerical approach applied to three-dimensional fault models in the Roer valley rift system (southeast Netherlands). Journal of Geophysical Research 109, B02401. http://dx.doi.org/10.1029/2003JB002586.
Yamanaka, Y., Kikuchi, M., 2004. Asperity map along the subduction zone in northeastern Japan inferred from regional seismic data. Journal of Geophysical Research 109, B07307. http://dx.doi.org/10.1029/2003JB002683.
Yoshida, K., Hasegawa, A., Okada, T., Iinuma, T., Ito, Y., Asano, Y., 2012. Stress before and after the 2011 great Tohoku-oki earthquake and induced earthquakes in inland areas of eastern Japan. Geophysical Research Letters 39, L03302. http://dx.doi.org/10.1029/2011GL049729.
Zalohar, J., Vrabec, M., 2010. Kinematics and dynamics of fault reactivation: the Cosserat approach. Journal of Structural Geology 32, 15–27.
Zhao, D., Huang, Z., Umino, N., Hasegawa, A., Kanamori, H., 2011. Structural heterogeneity in the megathrust zone and mechanism of the 2011 Tohoku-oki earthquake (M_w 9.0). Geophysical Research Letters 38, L17308. http://dx.doi.org/10.1029/2011GL048408.